Available online at www.sciencedirect.com

SciVerse ScienceDirect

Ceramics International 38 (2012) 1167–1174

CERAMICS INTERNATIONAL

www.elsevier.com/locate/ceramint

Synthesis and post-annealing effects on the transport properties of thermoelectric oxide $(ZnO)_mIn_2O_3$ ceramics

L.M. Wang [a,*], Ching-Yu Chang [b], Shau-Tin Yeh [b], Shinn Wei Chen [b], Zi An Peng [b], Shun Chang Bair [b], D.S. Lee [b], F.C. Liao [c], Y.K. Kuo [d,**]

[a] Graduate Institute of Applied Physics, National Taiwan University, Taipei 10617, Taiwan
[b] Department of Electrical Engineering, Da-Yeh University, Chang-Hwa 515, Taiwan
[c] Department of Materials Science and Engineering, Da-Yeh University, Chang-Hwa 515, Taiwan
[d] Department of Physics, National Dong Hwa University, Hualien 97401, Taiwan

Received 10 November 2010; received in revised form 25 May 2011; accepted 27 June 2011
Available online 1 September 2011

Abstract

The synthesis and transport properties of *n*-type thermoelectric oxide $(ZnO)_mIn_2O_3$ (Z_mIO) ceramics prepared by conventional solid-state reaction method have been reported. It is found that the transport properties of Z_mIO ceramics are very sensitive to the post-annealing temperature as well as the zinc content *m*. The resistivity of Z_5IO annealed at 1400 °C decreases by more than 2 orders of magnitude in comparison with that of Z_5IO annealed at 1200 °C, while the resistivities of Z_6IO compounds annealed at 1250 and 1350 °C are more than 3 orders of magnitude larger than that of Z_6IO annealed at 1300 °C. All the Z_mIO compounds annealed at 1300 °C show electron-type conduction with a lowest resistivity at $m = 6$. It is suggested that the oxygen defects or vacancies in the InO_2 layers play a major role on the carrier scattering mechanism, and the observed temperature-dependent resistivity for Z_5IO and Z_6IO compounds can be satisfactorily described by the variable-range hopping conduction. Furthermore, it is found that the values of Seebeck coefficient for Z_mIO are also very sensitive to the zinc content *m*. The dimensionless figure of merit of 0.0045 at 300 K for $m = 6$ has been obtained.

Keywords: C. Electrical properties; Thermoelectric properties; $(ZnO)_mIn_2O_3$ ceramics; Transparent conducting oxide

1. Introduction

Ceramic compounds $(ZnO)_mIn_2O_3$ (Z_mIO) have been widely exploited as alternative transparent conducting oxides [1,2] or thermoelectric materials [3,4]. It has been recently proposed that the Z_mIO compounds with suitable dopants exhibit superior electrical/optical properties, being a promising alternative to indium–tin oxide [5]. In addition, it has been demonstrated that the yttrium-substituted Z_5IO compounds showed a figure-of-merit value of 0.33 at 1073 K, a relatively high value among the *n*-type thermoelectric oxides [6]. A series of Z_mIO ($m = 2$–5 and 7) compounds were first prepared by Kasper and demonstrated the formation of these oxides at 1100–1550 °C [7]. Kimizuka and co-workers have systematically clarified the structure of a series of $InMO_3(ZnO)_m$ (M = Fe, Ga, Al and so on) and pointed out that this class of materials is isostructural to that of $LuFeO_3(ZnO)_m$ [8]. In addition, Ohta et al. have reported synthesis and electrical properties of Z_mIO ceramics [9]. Further, single crystalline thin film growth has been reported in several articles [10–12]. For the radio-frequency-sputtered thin films of Z_5IO, the lowest resistivity of 1.3×10^{-3} Ω cm with a wide band gap of 3.12 eV was obtained [11]. This stimulates the utilizations of Z_mIO compounds on transparent electrodes or photoelectric devices [1,12]. However, most of the attainable transport properties of conducting ceramic compounds are limited by the intrinsic properties of the materials used, such as the crystalline structure, doping contents, or the oxygen vacancies. It has been shown that the annealing condition is crucial on determining the crystalline quality, the defect diffusion, or the oxygen vacancies of ZnO compounds [13,14]. For example, the lowest

* Corresponding author. Tel.: +886 2 33665097; fax: +886 2 23639984.
** Corresponding author. Tel.: +886 3 8633697; fax: +886 3 8633690.
E-mail addresses: liminwang@ntu.edu.tw (L.M. Wang), ykkuo@mail.ndhu.edu.tw (Y.K. Kuo).

0272-8842/$36.00
doi:10.1016/j.ceramint.2011.06.068

resistivity of 6.2×10^{-4} Ω cm for InZnO films was obtained by annealing at 200 °C in a N_2 + 10% H_2 atmosphere [15]. It has also been reported that the resistivity, carrier concentration, and Hall mobility of Z_5IO films depend strongly on the annealing temperature and ambient atmosphere [11]. In this paper, we present the synthesis of Z_mIO ceramics prepared by conventional solid-state reaction method. It is found that the transport properties of Z_mIO ceramics are very sensitive to the post-annealing temperature as well as the zinc content m.

2. Experiment

Polycrystalline samples of Z_mIO (m = 4–6) were synthesized by a conventional solid-state reaction method using the starting materials of ZnO and In_2O_3 powders. Materials with stoichiometric ratios were ground and reacted at 1150 °C for 6 h in air. The obtained powders were reground, pressed into pellets under a pressure of 100 MPa, and heated in air again at annealing temperatures of 1200–1400 °C for 3 h. These pellets were placed in a sacrificial powder bed of the same composition to diminish the Zn loss. This procedure was repeated and the samples were finally cooled to room temperature at the rate of 5 °C/min. The X-ray powder diffraction (XRD) data were collected from 20° to 80° with a 2θ step of 0.01° using a diffractometer (Shimazu XRD6000, Japan) with Cu K_α radiation. The scanning electron microscope (SEM, Hitachi S-3000N) was used to characterize the surface morphologies of samples. The atomic ratios of Zn/In were determined by an energy dispersive spectrometer (EDS) using an EMAX system detector attached to the SEM for the assurance of sample compositions. The resistivity and carrier concentration were obtained by the standard dc four-terminal method and by Hall measurement, respectively. The bulk density of the pellets, determined by the Archimedes method, was 74–79% of the theoretical density and slightly increased with an increase in the post-annealing temperature. The resistivity of a given pellet was calculated by considering its relative density to give an approximate correction for this variation in sample density, as will be discussed in later section. Seebeck coefficient and thermal conductivity measurements were simultaneously carried out, by a direct heat pulse technique, in a helium closed cycle refrigerator over the temperature range of 10–400 K. Details of the thermal measurements have been reported elsewhere [16].

3. Results and discussion

Fig. 1 shows the X-ray diffraction spectra of Z_5IO prepared with different annealing temperatures. The obtained diffraction spectra are consistent with the expected hexagonal crystal structure [17]. It is noted that the impurity phase of In_2O_3 was detected in Z_5IO with annealing temperatures T_a below 1250 °C. The same situation is also observed for the Z_6IO samples, as shown in Fig. 2. Fig. 3 shows the $\theta - 2\theta$ X-ray diffraction spectra of Z_mIO (m = 4–6) prepared with annealing temperature of 1300 °C. Here we adopt the pseudo-$R3m$ crystalline cell for all samples to conveniently make the

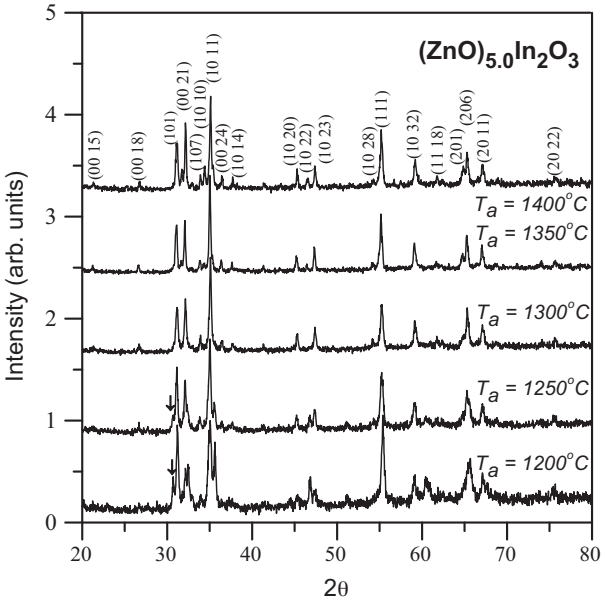

Fig. 1. X-ray diffraction spectra of Z_5IO prepared with different annealing temperatures. The arrows indicate the impurity phases of In_2O_3.

comparisons. It is clearly seen that the In_2O_3 impurity phase only appears in Z_4IO with T_a = 1300 °C. The appearance of In_2O_3 indicates an In-rich state in these annealing conditions for Z_mIO compounds. The intensity of the strongest impurity peaks observed in these X-ray diffraction data is below 5% of the main phase. The influence of impurity phases on the transport properties is thought to be negligible due to the insulating nature of In_2O_3. Fig. 4 shows the lattice parameters and the unit cell volume V_{cell} as a function of T_a for Z_5IO and Z_6IO ceramic compounds. As shown in Fig. 4, the lattice parameters a and c, and the unit cell volume V_{cell} increase slightly as T_a is increased from 1200 to 1400 °C for both Z_5IO and Z_6IO compounds. This indicates that the annealing process does not lead to a strong

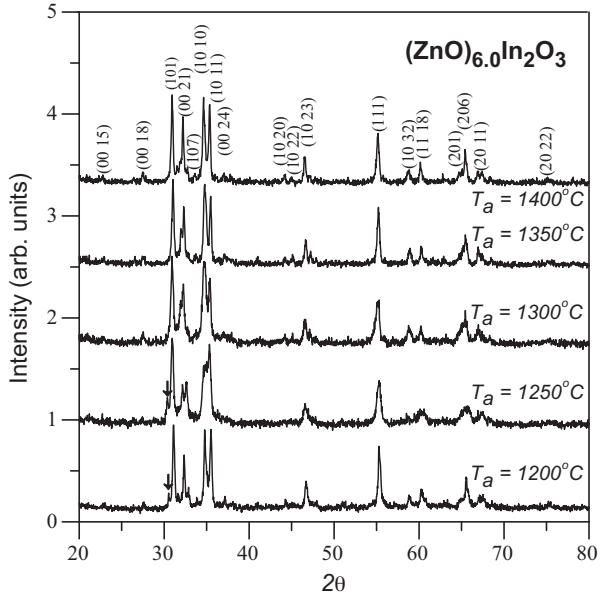

Fig. 2. X-ray diffraction spectra of Z_6IO prepared with different annealing temperatures. The arrows indicate the impurity phases of In_2O_3.

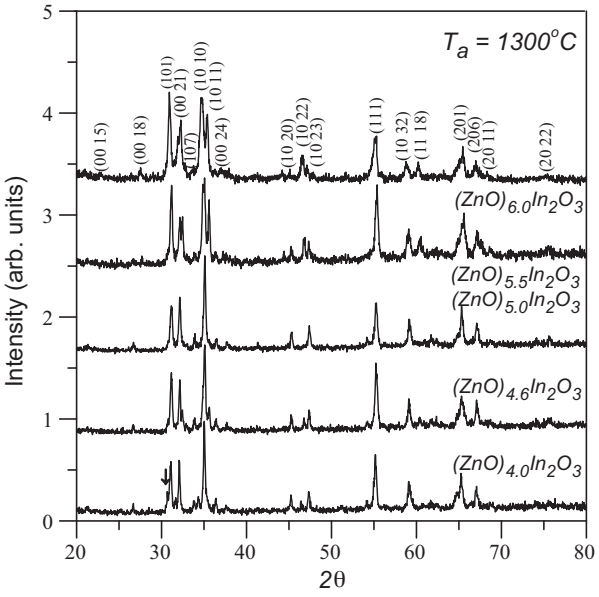

Fig. 3. X-ray diffraction spectra of Z_mIO prepared with annealing temperature of 1300 °C. The arrow indicates the impurity phases of In_2O_3 in Z_4IO.

distortion of crystal structure. Fig. 5 shows the lattice parameters and V_{cell} as a function of Zn concentration m of Z_mIO compounds. It is noted that the lattice parameters a and c, and V_{cell} decrease monotonously with increasing Zn concentration. The decrease of lattice parameters and V_{cell} can be attributed to a smaller ionic radius of Zn in these compounds. Since the ionic radius of Zn^{2+} (0.74 Å) is smaller than that of In^{3+} (0.81 Å) [18], the substitution of Zn ions into Z_mIO is expected to result in a reduction of the lattice parameters and V_{cell}.

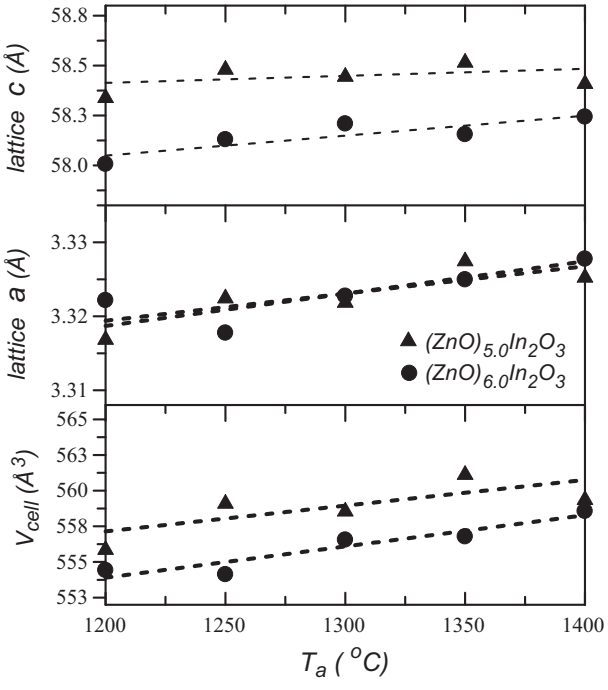

Fig. 4. Lattice parameters and the unit cell volume V_{cell} as a function of annealing temperature for Z_5IO and Z_6IO ceramic compounds.

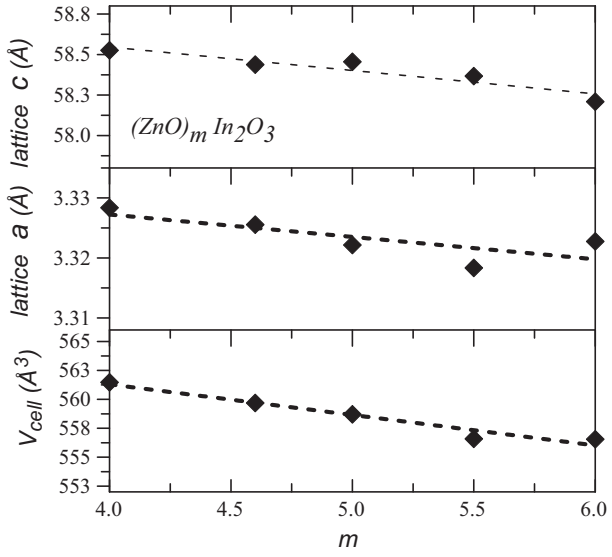

Fig. 5. Lattice parameters and V_{cell} as a function of Zn concentration m of Z_mIO compounds.

Fig. 6(a) and (b) show the temperature dependence of resistivity, ρ, for Z_5IO and Z_6IO ceramic compounds with different annealing temperatures, respectively. As previously mentioned, the resistivity of a given sample was calculated by considering its relative density to give an approximate correction for this variation in sample. Here the Bruggeman symmetric equation [19], $\rho_{corrected} = (1 - 1.5f_p)\rho_{mearsured}$, was used to correct for porosity. Here f_p is the volume fraction of pores and can be derived from the measured relative density.

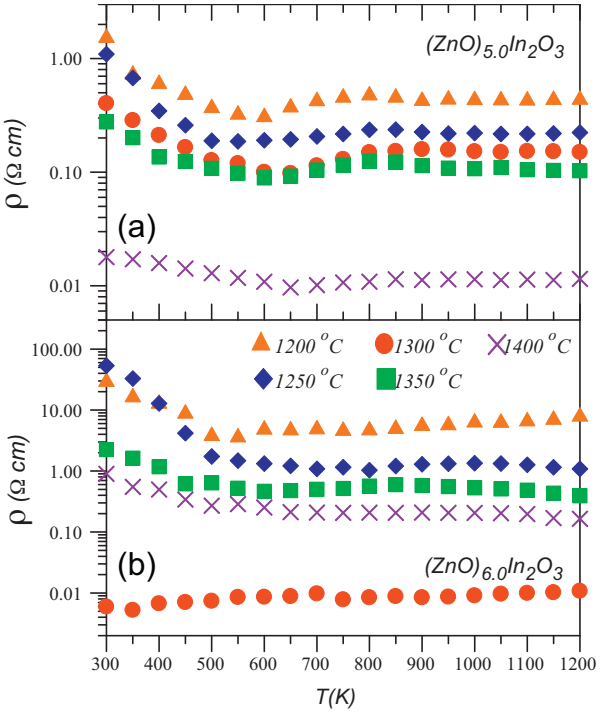

Fig. 6. Temperature dependence of resistivity for (a) Z_5IO and (b) Z_6IO ceramic compounds with different annealing temperatures. (For interpretation of the references to color in this figure legend, the reader is referred to the web version of the article.)

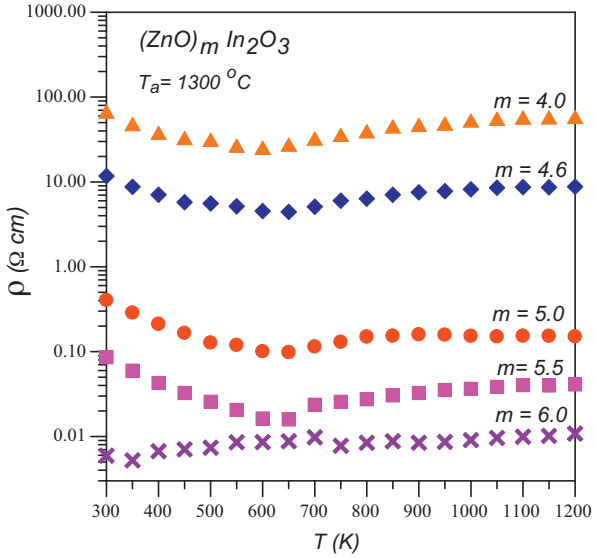

Fig. 7. Temperature dependence of resistivity for Z_mIO ceramic compounds annealed at 1300 °C. (For interpretation of the references to color in this figure legend, the reader is referred to the web version of the article.)

The corrected values of resistivity ($\rho_{corrected}$) are thus obtained and presented in this work. The resistivities of Z_5IO compounds show a local minimum at a temperature of around 600 K, and a lower resistivity value for Z_5IO with T_a of 1400 °C, as seen in Fig. 6(a). For Z_6IO compounds, the $\rho(T)$ curves, except that with T_a of 1300 °C, show a similar behavior as those of Z_5IO compounds. It is found that the Z_6IO annealed at 1300 °C has relatively a low resistivity, accompanying with a metallic-like behavior in the high temperature region. The $\rho(T)$ curves for Z_mIO compounds annealed at 1300 °C are shown in Fig. 7. As seen, the $\rho(T)$ curves, except that for $m = 6$, show a similar behavior as those of Z_5IO compounds. Fig. 8 and Fig. 9 show the correlation of room-temperature mobility μ, carrier concentration n, and resistivity ρ with T_a for Z_5IO and Z_6IO compounds, respectively. As can be seen, the Z_5IO compound annealed at 1400 °C shows the lowest resistivity of

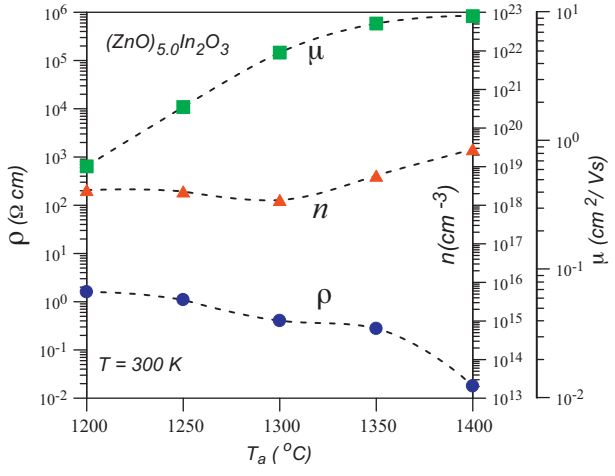

Fig. 8. Room-temperature mobility μ, carrier concentration n, and resistivity ρ versus T_a for Z_5IO compounds. (For interpretation of the references to color in this figure legend, the reader is referred to the web version of the article.)

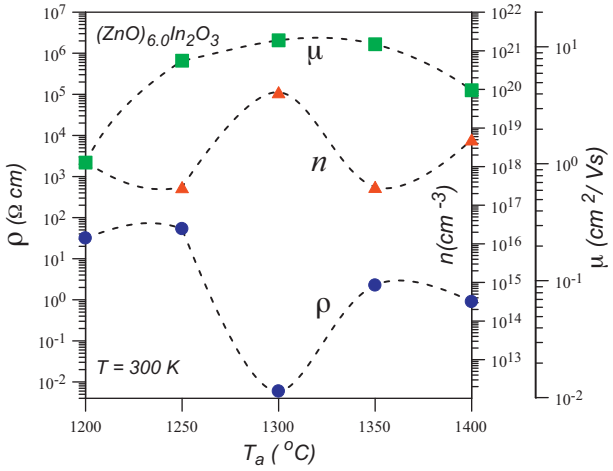

Fig. 9. Room-temperature mobility μ, carrier concentration n, and resistivity ρ versus T_a for Z_6IO compounds. (For interpretation of the references to color in this figure legend, the reader is referred to the web version of the article.)

1.79×10^{-2} Ω cm with larger values of mobility (9.2 cm^2/Vs) and carrier concentration (2.84×10^{19} cm^{-3}). On the other hand, the electrical property for Z_6IO compound is optimized with T_a of 1300 °C. A room-temperature resistivity of 5.94×10^{-3} Ω cm, mobility μ of 11.4 cm^2/Vs, and carrier concentration n of 8.5×10^{19} cm^{-3} are obtained, comparable to those reported elsewhere [3]. As seen in Fig. 8 and Fig. 9, the resistivity of Z_5IO annealed at 1400 °C decreases by more than two orders of magnitude in comparison with that of Z_5IO annealed at 1200 °C, while the resistivities of Z_6IO compounds annealed at 1250 and 1350 °C are more than three orders of magnitude larger than that of Z_6IO annealed at 1300 °C. These results indicate that the electrical properties of both Z_5IO and Z_6IO compounds are very sensitive to the annealing conditions. Fig. 10 shows the Zn-concentration dependences of μ, n, and ρ for Z_mIO compounds annealed at 1300 °C. All the Z_mIO compounds show consistently an electron-type conduction with the lowest resistivity when $m = 6$. The low value of resistivity for Z_6IO is presumably due to the increased carrier concentration and mobility in these oxides. However, such a result appears to be contrary to that observed by Moriga et al. [20], where an increase in resistivity with the content of Zn was reported. This discrepancy can be attributed to the different annealing or sintering temperatures used, indicating the annealing temperature plays an important role on the electrical properties of Z_mIO compounds. Further, SEM images for sintered surfaces of Z_5IO and Z_6IO compounds with different annealing temperatures are shown in Fig. 11(a)–(d), respectively. The SEM images reveal a spike-like microstructure for the high-conductivity Z_5IO and Z_6IO compounds annealed at 1400 and 1300 °C (see in Fig. 11(a) and (b)), whereas the SEM images show relatively small plate-like grains with many pores for the low-conductivity Z_5IO and Z_6IO compounds annealed at 1300 and 1200 °C (see Fig. 11(c) and (d) with a larger magnification). It is known that the electrical conductivity for a polycrystalline material can be affected by the grain size, grain boundary interfaces, and its intrinsic band structure. Thus, the

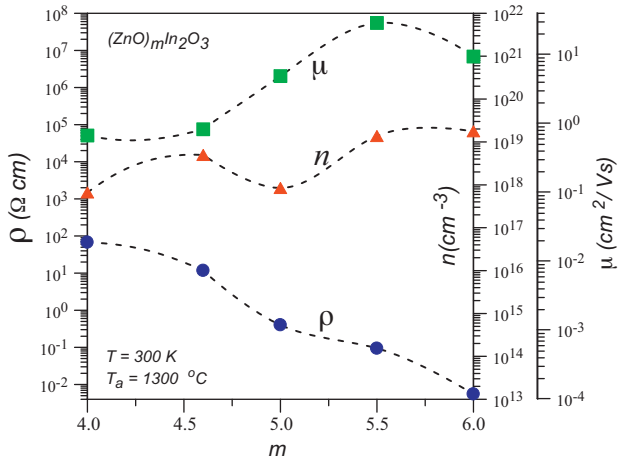

Fig. 10. Room-temperature mobility μ, carrier concentration n, and resistivity ρ versus T_a for Z_mIO compounds. (For interpretation of the references to color in this figure legend, the reader is referred to the web version of the article.)

present SEM results reveal a close connection between the morphology and electrical properties in these oxides.

Fig. 12(a) shows temperature dependent electrical resistivity for Z_5IO and Z_6IO compounds annealed at 1300 °C below 500 K, and the overall behavior of these samples is semiconducting in nature. The conduction mechanism of polycrystalline semiconductors is generally realized by the thermal activation process [21], grain boundary scattering [22], or variable-range hopping (VRH) conduction [23]. The first case can be expressed by $\rho(T) \propto \exp(E_a/k_BT)$, where E_a is the activation energy and k_B is the Boltzmann constant. It is evident that such an expression cannot be applied to the data, as shown in Fig. 12(b). The second case, which gives the dependence of $\rho(T) \propto T^{0.5}\exp(\phi_b/k_BT)$, can be examined by the relationship of $\ln(T^{-0.5}\rho)$ against T^{-1}. Here ϕ_b is the grain boundary potential barrier. As shown in Fig. 12(c), the conduction mechanism of Z_5IO and Z_6IO compounds does not follow the grain boundary scattering either. Hirano et al. [24] estimated the mean free paths of carriers, which was much smaller than the grain size of their Z_5IO samples, and excluded the grain boundary scattering as the origin of electrical transport mechanism. This is in accordance with our data analyses presented here. The third case predicts a temperature variation of electrical resistivity with the form $\rho(T) \propto T^{0.5}\exp[(T_0/T)^{1/4}]$, where T_0 is a characteristic temperature related to the distribution of localized electronic states. Fig. 12(d) shows the relationship of $\ln(T^{-0.5}\rho)$ against $T^{-1/4}$ for Z_5IO and Z_6IO compounds. As can be seen, a good linearity at temperatures between 100 and 400 K confirms the variable-range hopping conduction for Z_5IO and Z_6IO compounds. A detail carrier transport mechanism of $InGaO_3(ZnO)_5$ films has been reported by Nomura et al. [25]. They also found a variable-range-hopping-like conduction behavior of this material, indicating that these $InMO_3(ZnO)_m$ (M = In, Ga) compounds contains random potential barriers formed around conduction band edge. The dominating conduction mechanism, being the so-called hopping conduction of localized carriers between the oxygen-defect donors via percolation paths, is expected to be correlated with the average hopping distance of the carriers between localized states, which is similar to that of H_2-annealed ZnO films [26]. We thus conclude that the variation of electrical resistivity in these Z_5IO

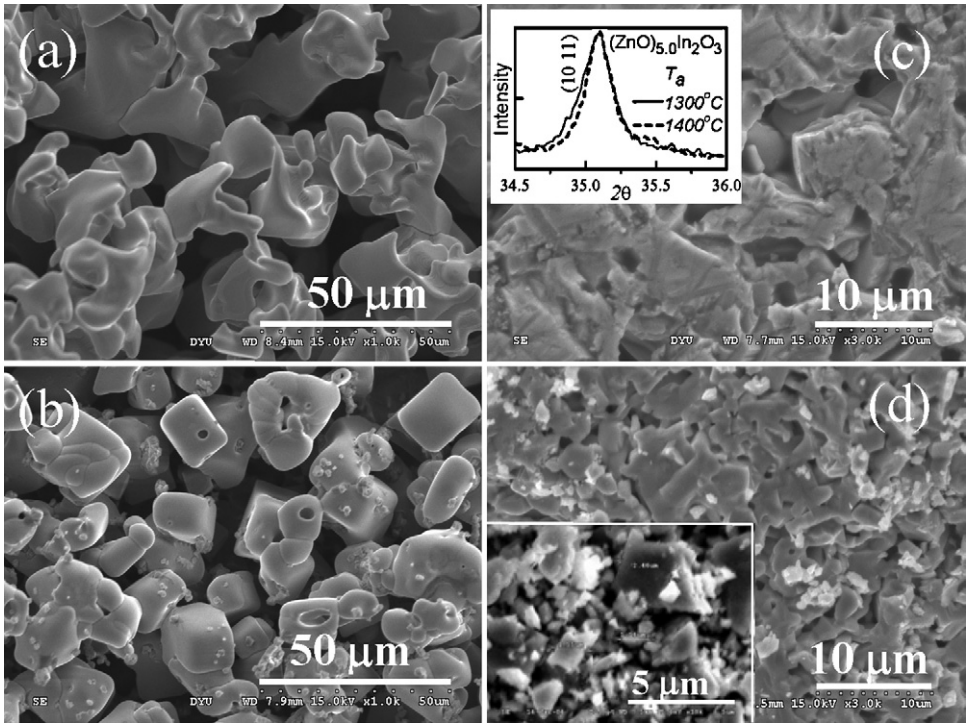

Fig. 11. SEM images for sintered surfaces of (a) Z_5IO annealed at 1400 °C, (b) Z_6IO annealed at 1300 °C, (c) Z_5IO annealed at 1300 °C, and (d) Z_6IO annealed at 1200 °C. The inset in (c) shows the X-ray diffraction spectra near the (1 0 1 1) peaks for Z_5IO annealed at 1400 and 1300 °C. The inset in (d) shows the image for Z_6IO annealed at 1350 °C.

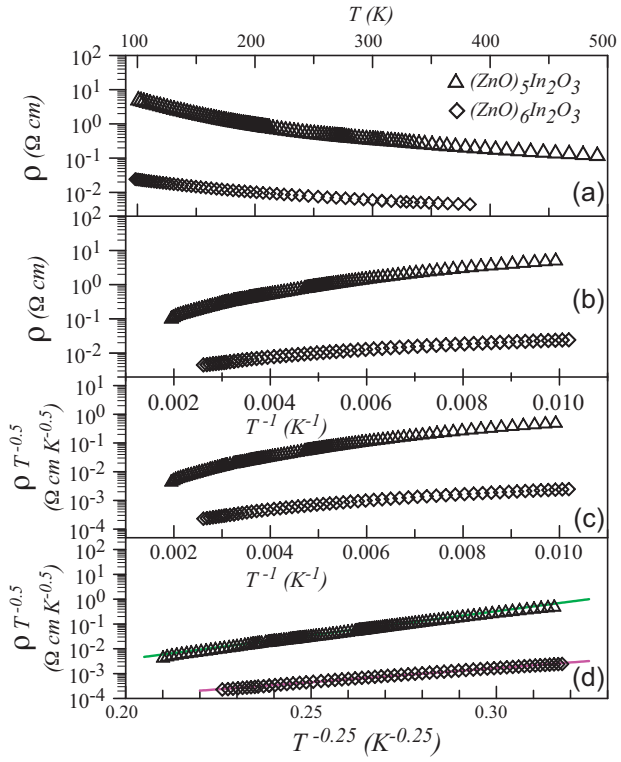

Fig. 12. The plots of (a) $\ln(\rho)$ versus T, (b) $\ln(\rho)$ versus T^{-1}, (c) $\ln(\rho T^{-0.5})$ versus T^{-1}, and (d) $\ln(\rho T^{-0.5})$ versus $T^{-0.25}$ for Z_5IO and Z_6IO compounds annealed at 1300 °C. Solid lines are the fitted curves. (For interpretation of the references to color in this figure legend, the reader is referred to the web version of the article.)

and Z_6IO compounds is most likely VRH kind, originates from the competition between the potential energy and the hopping distance of the charge carriers. Additionally, according to the electrical transport mechanism dominated by the oxygen-defect donors, we can review the effects of annealing temperature on the electrical properties of Z_5IO and Z_6IO compounds. We infer that the oxygen vacancies or the oxygen-defect donors will increase with the increase in annealing temperature, resulting in the increased conductivity and mobility for the *n*-type conductive Z_5IO and Z_6IO compounds. However the anomalous behavior of decreased conductivity and mobility observed on Z_6IO annealed at temperatures above 1350 °C (shown in Fig. 9) is possibly due to the smaller grain size (<2.5 μm) as seen in the inset of Fig. 11(d). It has been shown that an increase in the boundary area between grains due to a decrease in the particle size will result in a decrease in the carrier mobility for InZnO films [15]. The crystallite size was also calculated using Scherrer's equation: $D = 0.94\,\lambda/(\beta \cdot cos\theta)$, where D is the grain size, λ is the wavelength of the X-ray radiation used, β is the full width at half maximum of the diffraction peak, and θ is the Bragg diffraction angle of the peak. As shown in the inset of Fig. 11(c), the values of β of the most-intensity (1 0 1 1) diffraction peak for Z_5IO annealed at 1400 and 1300 °C are 0.220 and 0.275°, corresponding to the D values of 39.6 and 31.6 nm, respectively. The grain sizes are estimated to be in the range of 22.1–39.6 nm for all samples and decrease slightly with an increase in T_a. The estimated grain sizes are much smaller than those observed by the SEM, implying that the grains are formed by the aggregation of smaller crystallites in the samples. The small variation in the estimated grain size indicates that the electrical conductivity is little affected by the grain size. This result is consistent with the scenario that the dominating conducting mechanism for the electrical conductivity of our polycrystalline Z_mIO is the hopping conduction as discussed previously.

Fig. 13 shows temperature dependent Seebeck coefficient $S(T)$ of Z_mIO compounds annealed at 1300 °C between 10 and 400 K. The measured S was found to be negative in the entire temperature range we investigated, suggesting that the dominant carriers are electron-type in these compounds and being consistent with the Hall measurements. The largest room temperature value of $S = -242$ μV/K is observed for $m = 5.5$ which reduces with varying the value of m. For metals or semiconductors, the Seebeck coefficient is expected to be linear in temperature through the classical formula $S = (\pi^2 k_B^2/2e\varepsilon_F)T$, assuming a one-band model with an energy-independent relaxation time. Here, ε_F is the Fermi energy. However, the measured $S(T)$ curves for Z_mIO compounds exhibit a small upward concave curvature with increasing temperature. To account for this behavior and to separate the linear diffusive contribution from total $S(T)$, we have analyzed the $S(T)$ data with an empirical power law, $S(T) = AT + BT^3$. The first term represents the electronic diffusive contribution whereas the second term sets an upper bound to the contribution from electron–phonon normal processes [27]. The linear portion of S/T vs. T^2 plots shown

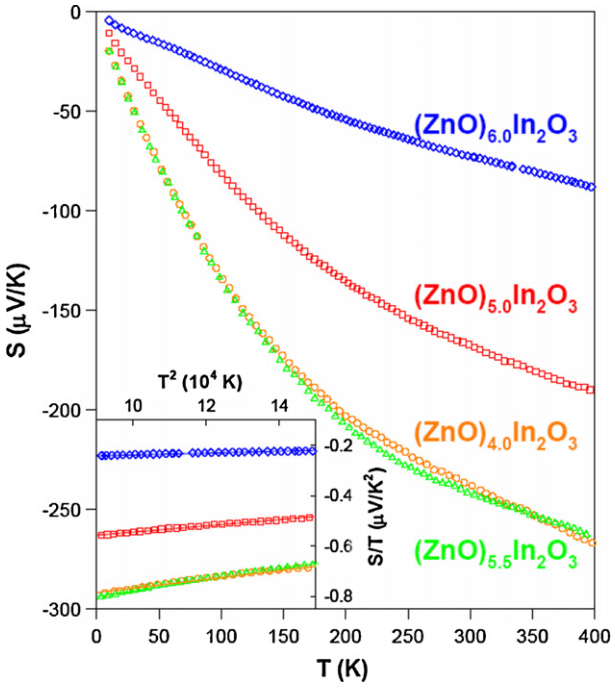

Fig. 13. The temperature-dependent Seebeck coefficient curves for Z_mIO compounds annealed at 1300 °C over the temperature range 10 K < T < 400. 400. Inset: a linear relation in the S/T vs. T^2 plot indicates that the $S(T)$ data roughly follow an empirical power law $S(T) = AT + BT^3$. (For interpretation of the references to color in this figure legend, the reader is referred to the web version of the article.)

in the inset of Fig. 13 exhibits the temperature range over which the proposed formula is valid. From the relation $A = \pi^2 k_B^2 / 2e\varepsilon_F$, we extracted the Fermi energy $\varepsilon_F = 0.04$ eV for $m = 4$ and 0.14 eV for $m = 6$. Such a result is connected to an enhancement of the metallic behavior in the Z_mIO compounds as increasing the m value, being consistent with the $\rho(T)$ data.

Fig. 14 shows temperature dependent thermal conductivity $\kappa(T)$ of Z_mIO compounds annealed at 1300 °C between 10 and 400 K. It should be noted here that the values of $\kappa(T)$ shown in the figure are corrected by considering the bulk density of each sample. The obtained room temperature value of $\kappa(300\ K) \sim 5$ W/m-K, relatively little affected with respect to the changes in the composition, is close to the reported results [9]. Generally, the total thermal conductivity for ordinary metals and semiconductors is a sum of electronic and lattice terms. The electronic thermal conductivity κ_e can be evaluated using the Wiedemann–Franz law $\kappa_e \rho / T = L$. Here ρ is the *dc*-electric resistivity and the Lorentz number $L = 2.45 \times 10^{-8}$ W Ω K^{-2}. We thus obtained the electronic thermal conductivity κ_e for the most conducting sample Z_6IO (at $T = 300$ K; the electrical resistivity $\rho_{300} \sim 6$ mΩ cm) as 0.03 W/m-K. From this estimation, one can safely argue that the total thermal conductivity is mainly due to the lattice phonons rather than the charge carriers, due to the high electric resistivity of these oxides.

It is noted that the measured value of κ is quite small and comparable to those of glassy materials [28]. For typical non-crystalline materials (bad metals), the magnitude of $\kappa(300\ K)$ lies in the range of 0.5–6.5 W/m-K. For a crystalline solid, such a low value of thermal conductivity can be thought to originate from random, noncentral distortions of the lattice, resulting in high degree of disorder. In the present case of the Z_mIO compounds, the low thermal conductivity can be associated with oxygen defects or vacancies in the InO_2 layers. At low temperatures, $\kappa(T)$ is followed by a well defined peak around 40 K in all samples. This feature is a typical behavior of solids and the maximum takes place at the temperature where the phonon mean free path is approximately equal to the crystal site distance, ascribed to the generalized Umklapp process. It should be mentioned here that the Z_5IO sample has the most pronounced peak among all samples, indicating a more ordered crystal structure for this particular compound. Further, it is found that $\kappa(T)$ increases with increasing temperature above the low-T peak. This is quite unusual since the high temperature thermal conductivity of the crystalline insulators is mostly a decreasing function of temperature and cannot be attributed to high temperature electron or phonon processes. Such a behavior of high-T κ (T) may be attributed to the local anharmonic lattice distortions associated with the formation of structural polarons. As a result of the presence of oxygen defects or vacancies in these oxides, these polarons are thermally excited that could provide an additional channel for the heat conduction at high temperatures.

Finally, from the electrical and thermal transport properties presented above, one can estimate the thermoelectric performance of these $(ZnO)_mIn_2O_3$ ceramics. It is found that the dimensionless figure of merit ZT is optimized for $m = 6$ with a value of 0.0045 at 300 K. This value is comparable with that reported earlier with $m = 9$ [9], however, two orders of magnitude lower than that of state of the art bismuth telluride-based thermoelectric materials at room temperature. The present work represents potential candidates for intermediate- and high-temperature thermoelectric applications with a careful selection of Zn content and annealing condition in the Z_mIO system.

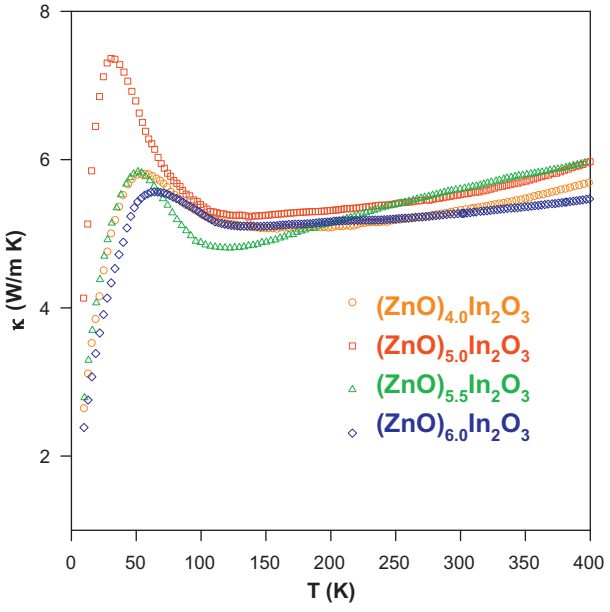

Fig. 14. The temperature-dependent thermal conductivity for Z_mIO compounds annealed at 1300 °C. (For interpretation of the references to color in this figure legend, the reader is referred to the web version of the article.)

4. Conclusion

In conclusion, the synthesis and transport properties of Z_mIO ceramics prepared by conventional solid-state reaction method have been studied. It can be seen that the lattice parameters of Z_mIO ceramics decrease monotonously with the increase in Zn concentration due to the smaller ionic radii of Zn in these compounds. On the other hand, the transport properties of Z_mIO ceramics are found to be very sensitive to the post-annealing temperature as well as the zinc content m. The Z_5IO compound annealed at 1400 °C shows a lower resistivity with larger values of mobility and carrier concentration, while Z_6IO compound annealed at 1300 °C achieves an optimum electrical property with a room-temperature resistivity value of 5.94×10^{-3} Ω cm. The resistivity of Z_5IO annealed at 1400 °C decreases by more than 2 orders of magnitude in comparison with that of Z_5IO annealed at 1200 °C, while the resistivities of Z_6IO compounds annealed at 1250 and 1350 °C are more than 3 orders of magnitude larger than that of Z_6IO annealed at 1300 °C. Moreover, all the Z_mIO compounds with a T_a of 1300 °C show a lowest resistivity at $m = 6$. In the analysis of temperature-dependent resistivity data, the conduction mechanism can be satisfactorily described by variable-range hopping model for Z_5IO and Z_6IO compounds. The measured

Seebeck coefficient was found to be negative in the entire temperature range we investigated, suggesting that the dominant carriers are electron-type in these compounds and being consistent with the Hall measurements. The measured room temperature value of thermal conductivity is about 5 W/m-K, relatively little affected with respect to the changes in the Zn concentration. It is inferred that the oxygen defects or vacancies in the InO_2 layers play an important role on both the electrical and thermal transport properties of these $(ZnO)_mIn_2O_3$ ceramics.

Acknowledgement

The authors thank the National Science Council of Taiwan for financial support under Grant Nos. NSC-98-2112-M-212-001-MY3 (LMW) and NSC-97-2628-M-259-001-MY3 (YKK).

References

[1] K. Ramamoorthy, K. Kumar, R. Chandramohan, K. Sankaranarayanan, Review on material properties of IZO thin films, Mater. Sci. Eng. B 126 (2006) 10–15.

[2] T. Moriga, T. Okamoto, K. Hiruta, A. Fujiwara, I. Nakabayashi, Structures and physical properties of films deposited by simultaneous DC sputtering of ZnO and In_2O_3 or ITO targets, J. Solid State Chem. 155 (2000) 312–319.

[3] H. Kaga, R. Asahi, T. Tani, Thermoelectric properties of doped $(ZnO)_mIn_2O_3$, Jpn. J. Appl. Phys. 43 (2004) 3540–3543.

[4] T. Tani, S. Isobe, W.-S. Seo, K. Koumoto, Thermoelectric properties of highly textured $(ZnO)_5In_2O_3$ ceramics, J. Mater. Chem. 11 (2001) 2324–2328.

[5] S.P. Harvey, T.O. Mason, D.B. Buchholz, R.P.H. Chang, Carrier generation and inherent off-stoichiometry in Zn, Sn Co doped, J. Am. Ceram. Soc. 91 (2008) 467–472.

[6] S. Isobe, T. Tani, Y. Masuda, W.-S. Seo, K. Koumoto, Thermoelectric performance of yttrium-substituted $(ZnO)_5In_2O_3$, Jpn. J. Appl. Phys. 41 (2002) 731–732.

[7] V.H. Kasper, Neuartige phasen mit wurtzitähnlichen strukturen im system ZnO–In_2O_3, Z. Anorg. Allg. Chem. 349 (1967) 113–123.

[8] N. Kimizuka, M. Isobe, M. Nakamura, Syntheses and single-crystal data of homologous compounds, $In_2O_3(ZnO)_m$ ($m = 3$, 4, and 5), $InGaO_3(ZnO)_3$, and $Ga_2O_3(ZnO)_m$ ($m = 7$, 8, 9, and 16) in the In_2O_3–$ZnGa_2O_4$–ZnO system, J. Solid State Chem. 116 (1995) 170–178.

[9] H. Ohta, W.-S. Seo, K. Koumoto, Thermoelectric properties of homologous compounds in the ZnO–In_2O_3 system, J. Am. Ceram. Soc. 79 (1996) 2193–2196.

[10] (a) K. Nomura, H. Ohta, K. Ueda, M. Orita, M. Hirano, H. Hosono, Novel film growth technique of single crystalline $In_2O_3(ZnO)_m$ (m = integer) homologous compound, Thin Solid Films 411 (2002) 147–151;
(b) D. Craciun, G. Socol, N. Stefan, M. Miroiu, Valentin, Craciun, Structural investigations of InZnO films grown by pulsed laser deposition technique, Thin Solid Films 518 (2010) 4564–4567.

[11] H. Hiramatsu, W.-S. Seo, K. Koumoto, Electrical and optical properties of radio-frequency-sputtered thin films of $(ZnO)_5In_2O_3$, Chem. Mater. 10 (1998) 3033–3039.

[12] T. Minami, T. Kakumu, Y. Takeda, S. Takata, Highly transparent and conductive ZnO–In_2O_3 thin films prepared by dc magnetron sputtering, Thin Solid Films 290–1 (1996) 1–5.

[13] J. Huang, H. Lu, Z. Ye, L. Wang, B. Zhao, H. He, Microstructure and defect investigations of the as-grown and annealed ZnO/Si thin films, J. Appl. Phys. 102 (2007) 053521.

[14] H.F. Liu, S.J. Chua, G.X. Hu, H. Gong, N. Xiang, Annealing effects on electrical and optical properties of ZnO thin-film, J. Appl. Phys. 102 (2007) 063507.

[15] C. Lee, W. Lee, H. Kim, H.W. Kim, Influence of annealing atmosphere on the structure, resistivity, and transmittance of InZnO thin films, Ceram. Int. 34 (2008) 1089–1092.

[16] C.S Lue, Y.K. Kuo, Thermoelectric properties of the semimetallic Heusler compounds $Fe_{2-x}V_{1+x}M$ (M = Al, Ga), Phys. Rev. B. 66 (2002) 085121.

[17] Y. Masuda, M. Ohta, W.-S. Seo, W. Pitschke, K. Koumoto, Structure and thermoelectric transport properties of lsoelectronically substituted $(ZnO)_5In_2O_3$, J. Solid State Chem. 150 (2000) 221–227.

[18] B. Joseph, P.K. Manoj, V.K. Vaidyan, Studies on preparation and characterization of indium doped zinc oxide films, Bull. Mater. Sci. 28 (2005) 487–493.

[19] D.S. McLachlan, M. Blaszkiewicz, R.E. Newnham, Electrical-resistivity of composites, J. Am. Ceram. Soc. 73 (1990) 2187–2203.

[20] T. Moriga, D.D. Edwards, T.O. Mason, Phase relationships and physical properties of homologous compounds, J. Am. Ceram. Soc. 81 (1998) 1310–1316.

[21] B.J. Lokhande, P.S. Patil, M.D. Uplane, Deposition of highly oriented ZnO films, Mater. Lett. 57 (2002) 573–579.

[22] J.Y.W. Seto, The electrical properties of polycrystalline silicon films, J. Appl. Phys. 46 (1975) 5247–5254.

[23] R.M. Hill, Hopping conduction in amorphous solids, Phil. Mag. 24 (1971) 1307–1325.

[24] S. Hirano, S. Isobe, T. Tani, N. Kitamura, I. Matsubara, K. Koumoto, Electric and thermal transport properties in layer-structured $(ZnO)_mIn_2O_3$, Jpn. J. Appl. Phys. 41 (2002) 6430–6435.

[25] K. Nomura, T. Kamiya, H. Ohta, K. Ueda, M. Hirano, H. Hosono, Carrier transport in transparent oxide semiconductor with intrinsic structural randomness probed using single-crystalline $InGaO_3(ZnO)_5$ films, Appl. Phys. Lett. 85 (2004) 1993–1995.

[26] Y. Natsume, H. Sakata, Electrical and optical properties of zinc oxide films post-annealed in H_2 after fabrication by sol–gel process, Mater. Chem. Phys. 78 (2002) 170–176.

[27] R.D. Bernard, Thermoelectricity in Metals and Alloys, Taylor & Francis Ltd, London, 1972, 136.

[28] D.W. Visser, A.P. Ramirez, M.A. Subramanian, Thermal conductivity of manganite perovskites: colossal magnetoresistance as a lattice-dynamics transition, Phys. Rev. Lett. 78 (1997) 3947–3950.